Characteristics of InGaP/InGaAs pseudomorphic high electron mobility transistors with triple delta-doped sheets

© Kuei-Yi Chu, Meng-Hsueh Chiang*,¶, Shiou-Ying Cheng*,¶¶, Wen-Chau Liu

Institute of Microelectronics, Department of Electrical Engineering, National Cheng-Kung University, Tainan, TAIWAN 70101, Republic of China
* Department of Electronic Engineering, National II an University, I-Lan, TAIWAN, Republic of China

(Получена 21 марта 2011 г. Принята к печати 28 июня 2011 г.)

Fundamental and insightful characteristics of InGaP/InGaAs double channel pseudomorphic high electron mobility transistors (DCPHEMTs) with graded and uniform triple δ-doped sheets are coomprehensively studied and demonstrated. To gain physical insight, band diagrams, carrier densities, and direct current characteristics of devices are compared and investigated based on the 2D semiconductor simulator, Atlas. Due to uniform carrier distribution and high electron density in the double InGaAs channel, the DCPHEMT with graded triple δ-doped sheets exhibits better transport properties, higher and linear transconductance, and better drain current capability as compared with the uniformly triple δ-doped counterpart. The DCPHEMT with graded triple δ-doped structure is fabricated and tested, and the experimental data are found to be in good agreement with simulated results.

1. Introduction

Over the several past years, applications of high electron mobility transistors (HEMTs) on high speed digital and microwave circuits have been widely investigated [1–4]. Generally, a wide gate voltage swing is required for the linear amplifier application. However, an important but undesired charecteristic of these devices is the presence of the parallel conductance. The onset of parallel conductance in the wide bandgap doping layer leads to a sharp peak in transconductance, which becomes a limitation for linear operation as well as the current driving capability. Thus, in order to overcome these drawbacks of conventional HEMTs, some device structures and theoretical analyses were proposed [5–7]. Hsu et al. [8] demonstrated that GaAs/InGaAs/GaAs pseudomorphic high electron mobility transistor (PHEMT) with symmetric double δ-doped sheets exhibits a broad transconductance plateau region. In addition, Kao et al. [9] shown that multi-couple δ-doped GaAs/InGaAs/GaAs double channel pseudomorphic heterojunctions field effect transistor (PHFET) gives higher sheet carrier density and mobility and higher current driving capability as compared to conventional HFETs. Based on these device structures, high current drive capability and high carrier density can be expected. Therefore the linearity properties and microwave performance could also be further improved.

In this work, we propose InGaP/InGaAs double channel pseudomorphic high electron mobility transistors (DCPHEMTs) with graded and uniform truple δ-doped sheets in this work. The theoretical analysis and simulation are done by using a 2D semiconductor simulator ATLAS [10,11] from SILVACO. The band diagrams, carrier transport properties, and DC (direct current) characteristics of devices are presented and compared. In addition, a practical DCPHEMT with graded triple δ-doped sheets structure is fabricated and studied. Good DC and microwave performances of the studied devices are obtained. Furthermore, the simulated data are in good agreement with experimental results.

2. Model and device Structure

The layer structures of simulated DCPHEMT devices are shown in Table. The device structure layers consisted of a 5000 Å GaAs buffer, a 450 Å $In_{0.49}Ga_{0.51}P$ buffer, a δ-doped sheet with the doping density of $\delta_3(n^+)$, a 50 Å $In_{0.49}Ga_{0.51}P$ spacer, a 100 Å $In_{0.2}Ga_{0.8}As$ channel, a 40 Å GaAs spacer, a δ-doped sheet with the doping density of $\delta_2(n^+)$, a 40 Å GaAs spacer, a 100 Å $In_{0.2}Ga_{0.8}As$ channel, a 50 Å $In_{0.49}Ga_{0.51}P$ spacer, a δ-doped sheet with the doping density of $\delta_1(n^+)$, a 160 Å $In_{0.49}Ga_{0.51}P$ barrier layer, and a 300 Å n^+-GaAs ($n^+ = 4 \cdot 10^{18}\,cm^{-3}$) cap layer. For comparison, graded ($\delta_1(n^+) = 3 \cdot 10^{12}$, $\delta_2(n^+) = 2 \cdot 10^{12}$ and $\delta_3(n^+) = 1 \cdot 10^{12}\,cm^{-2}$) and uniform ($\delta_1(n^+) = \delta_2(n^+) = \delta_3(n^+) = 2 \cdot 10^{12}\,cm^{-2}$) triple δ-doped sheets are employed in device A and B, respectively. A 2D semiconductor simulation package ATLAS was used to analyze the energy band diagrams, carrier distribution, and DC characteristics of the studied devices in this work. Five fundamental equations related to electron and hole current continuity, electron and hole concentrations and the Poisson equation were taken into account to simulate device performances. Other important physical mechanisms were also included in this study, such as Boltzmann statistics, Shockley–Read–Hall (SRH) recombination, field-dependent mobility, and consentration-dependent mobility. For considerable accuracy, in the calculation process we used a total triangle unit number up to 21712 and total grid points up to 15113. Furthermore, in order to confirm our theoretical analyses, a practical DCPHEMT with graded triple δ-doped sheets (device A) was fabricated for compari-

¶ E-mail: mhchiang@niu.edu.tw
¶¶ E-mail: sycheng@niu.edu.tw

The different InGaP/InGaAs HEMT structures used in the theoretical calculation

Layer	Material	Doping type and level (cm^{-3})	Width (Å)	Device	
				A	B
Cap	GaAs	$n^+ = 3 \cdot 10^{18}$	300		
Schottky	$In_{0.49}Ga_{0.51}P$	Undoped	160		
$\delta_1(n^+)$	...	...	...	$n^+ = 3 \cdot 10^{12}$ cm^{-2}	$n^+ = 2 \cdot 10^{12}$ cm^{-2}
Spacer	GaAs	Undoped	50		
Channel	$In_{0.2}Ga_{0.8}As$	≪	100		
Spacer	GaAs	≪	40		
$\delta_2(n^+)$	...	...	...	$n^+ = 2 \cdot 10^{12}$ cm^{-2}	$n^+ = 2 \cdot 10^{12}$ cm^{-2}
Spacer	GaAs	Undoped	40		
Channel	$In_{0.2}Ga_{0.8}As$	≪	100		
Spacer	$In_{0.49}Ga_{0.51}P$	≪	50		
$\delta_3(n^+)$	...	...	...	$n^+ = 1 \cdot 10^{12}\,cm^{-2}$	$n^+ = 2 \cdot 10^{12}\,cm^{-2}$
Buffer	$In_{0.49}Ga_{0.51}P$	Undoped	450		
≪	GaAs	≪	5000		
		S.I. GaAs Substrate			

son. For practical device fabrication, the drain/source ohmic contacts were formed on the n^+-GaAs cap layer by evaporating AuGe/Ni/Au metals and alloyed at 350°C for 30 s. After that, the n^+-GaAs cap layer was etched by wet etching. The dielectric spin-on-glass (SOG) thickness is 1 μm [12]. Then, the gate window with length of 1 μm was defined using photoresist and re-flowed by a baking process at 140°C for 1 min. After reflow the gate window length $L_g = 0.8\,\mu$m. Finally, the gate Schottky contact was produced by the thermal evaporation of Au metal on the undoped InGaP Schottky barrier layer. The gate dimension, source-gate and source-drain separation of the simulated and experimental devices are $0.8 \times 100\,\mu m^2$, 3 and 7 μm, respectively.

3. Results and Discussion

The schematic band diagrams of simulated devices A and B are shown in Fig. 1, *a* and 1, *b*, respectively. The applied gate-source voltage V_{GS} is swept from −2 to 2 V with 0.5 V per step. The reference origin of the depth axis is defined as the top position of the InGaP barrier layer. For device B, the δ-doping $\delta_1(n^+)$ is lower than that in device A. The conduction band diagrams of the studied device B show upward tendency within the upper channel and Schottky barrier layers. As a result, simulations show conduction band within double InGaAs channel layers of device A is flatter than that of device B. Therefore, the device A could be expected to obtain a more uniform electron distribution and higher electron density in the double InGaAs channel layers. The corresponding calculated electron densities for the simulated devices A and B are shown in Fig. 2, *a* and 2, *b*, respectively. Obviously, the electron densities of both devices can neglected realistically at $V_{GS} = -1.5$ V. It means that the device is operated under off status. In contrast, when the applied V_{GS} is higher than −0.5 V, the devices are operated under the conducting state. In addition, due to the employed graded triple δ-doped sheets, the simulated device A exhibits a more uniform carrier distribution and higher electron density in double InGaAs channel layers than those of device B. Note that the electron density of device A is slightly higher than that of device B over the entire biased regimes, implying that the simulated device A could be expected to obtain higher current drive capability, higher transconductance and greater device linearity characteristics.

Typical common-source ouptup current-voltage (*I-V*) characteristics of simulated devices A and B and experimental device are shown in Fig. 3, where symbols denote characteristics of the experimental device. The applied gate−source voltage V_{GS} is swept from 1.5 to −2 V in −0.5 V steps. Clearly, due to the high Schottky barrier height and good carrier confinement, the devices can be operated under higher V_{GS} of +1.5 V without significant gate leakage current. Good saturation and pinch-off properties are found for both devices. Moreover, the so-called parallel conduction and transconductance suppression, which are usually observed in traditional HEMTs, are not found in our studied devices. Furthermore, the higher drain current is sound in simulated device A. The available drain saturation current I_{DS} values of 411, 343 and 408 mA/mm are obtained for device A, device B and experimental device at $V_{GS} = +1.5$ V, respectively. In addition, the simulated data generally agree with experimentally measured results and confirm that the employed appropriate triple δ-doped densities indeed plays an important role in device behavior.

The corresponding I_{DS} and transconductance g_m versus V_{GS} are shown in Fig. 4. The drain−source voltage is fixed at $V_{DS} = 3.5$ V. It can be seen that the device A shows relatively better linear properties and higher transconductance. The maximum values of transconductance $g_{m,\max}$

are 177, 159 and 175 mS/mm for deivce A, device B and experimental device, respectively. Furthermore, the corresponding flat and wide V_{GS} operation regimes, defined as 90% from $g_{m,max}$, are 1.33, 1.05 and 1.7 V, respectively. Charly, the simulated curves fit quite well with experimental results under the biased range of $-0.6 \leqq V_{GS} \leqq 1.8$ V. In addition, in order to further investigate the linearitiy properties of the studied devices, a sixth, order polynomial equation is employed. The polynomial coefficients can be expressed as follows [13]:

$$I_{DS} = a_0 + a_1 V_{GS} + a_2 V_{GS}^2 + a_3 V_{GS}^3 + a_4 V_{GS}^4 + a_5 V_{GS}^5 + a_6 V_{GS}^6, \quad (1)$$

where a_0 is I_{DSS} values at $V_{GS} = 0$ and a_n (n from 1 to 6) are independent coefficients to determine the device

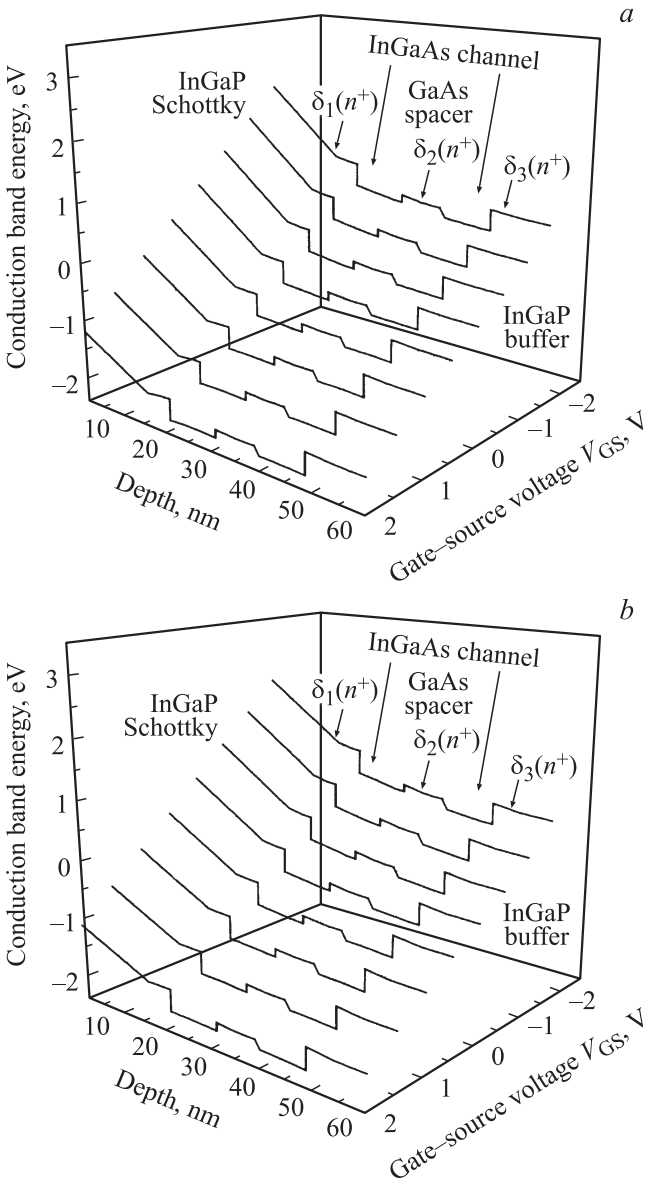

Figure 1. Energy band diagrams of the simulated devices: *a* — A and *b* — B.

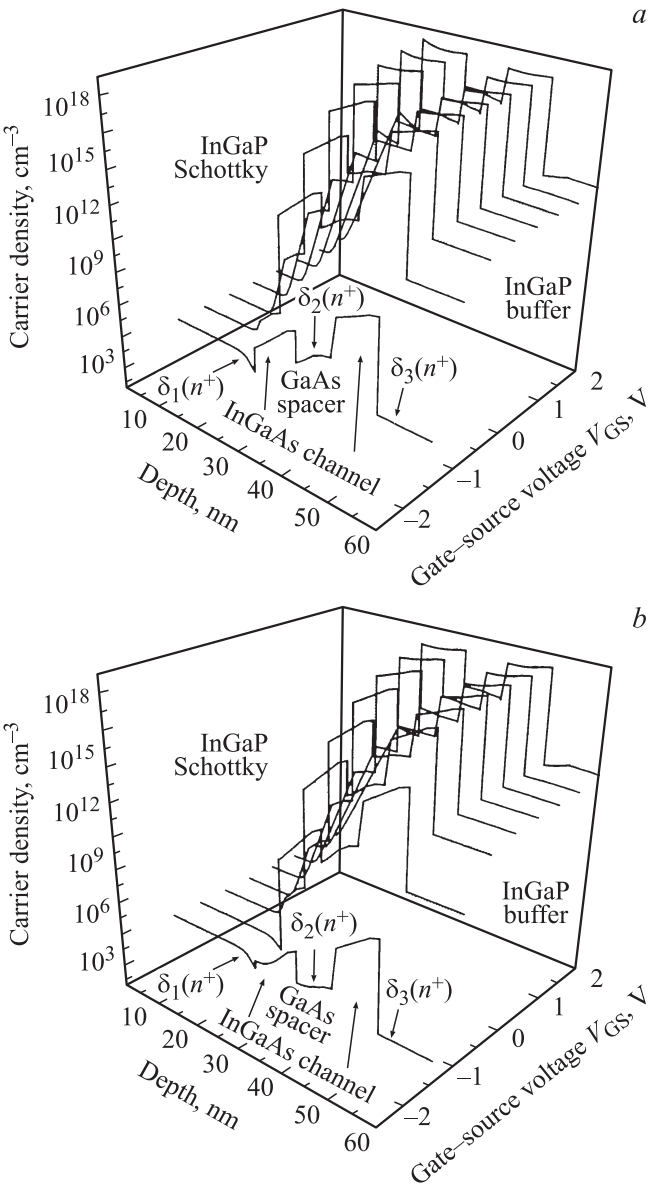

Figure 2. Calculated electron densities of the simulated devices: *a* — A and *b* — B.

linearity properties. For a better linearity of devices, the higher-order $|a_n/a_1|$ ($n \geq 2$) should be minimized. The coefficients of devices extracted from the simulated data are listed in the inset of Fig. 4. Apparently, the device A reveals relatively better linear properties and higher I_{DSS} than those of the device B. The I_{DSS} are 137.56 and 100.15 mA/mm for device A and B, respectively. According to the device simulation results, device A has more uniform carrier distribution and higher electron density in the double InGaAs channel than in device B when biased. This can explain why device A has a better linearity, higher I_{DSS} and higher $g_{m,max}$.

The experimental microwave performance of the studied device is shown in Fig. 5. The measured experimental results were measured by an HP8510C network analyzer in

confunction with cascade probs. Under the bias condition of $V_{DS} = 3.5$ V, the maximum unit current gain cut-off frequency f_T and f_{max} are 17.3 and 35.1 GHz, respectively. Note that the flat and wide V_{GS} operating regimes, for both f_T and f_{max} above 80% of peak values, are over 2 V, leading to a substantial advantage of DCPHEMT with graded triple δ-doped sheets in high-frequency circuit applications.

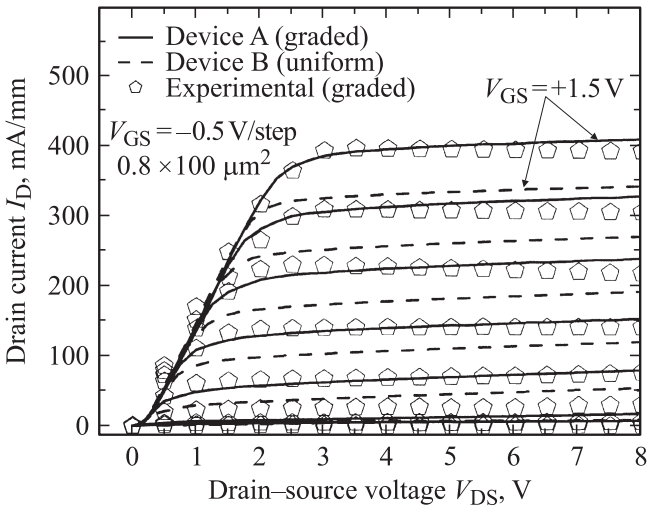

Figure 3. Comparisons of simulated and experimental common-source output *I-V* characteristics.

	Device A	Device B
a_0	137.56	100.151
a_1	159.1019	136.6899
$\lvert a_2/a_1\rvert$	0.0109	0.2573
$\lvert a_3/a_1\rvert$	0.021	0.1085
$\lvert a_4/a_1\rvert$	0.0139	0.0217
$\lvert a_5/a_1\rvert$	0.0352	0.0695
$\lvert a_6/a_1\rvert$	0.0099	0.0124

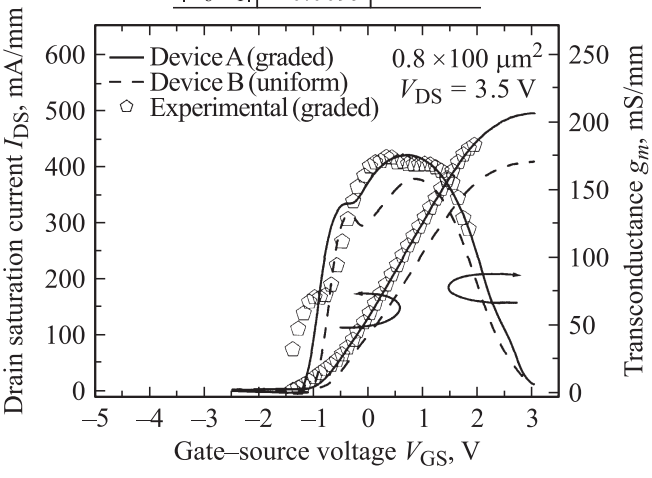

Figure 4. The relationships between the drain saturation current I_{DS}, transconductance g_m and gate–source voltage V_{GS}.

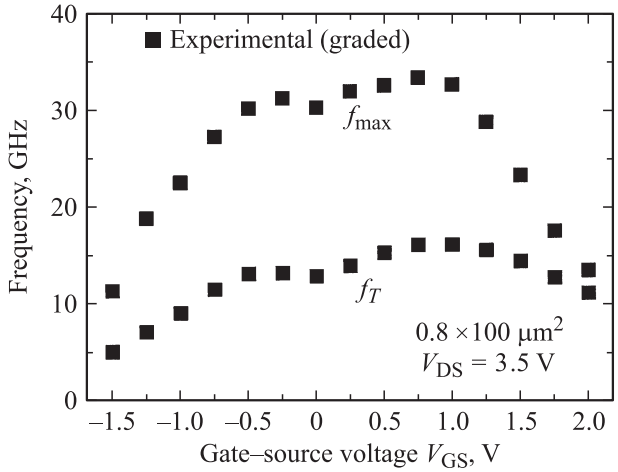

Figure 5. The relationships between unit current gain cut off frequency f_T, maximum oscillation frequency f_{max} and gate–source voltage V_{GS}.

4. Conclusion

In conclusion, the characteristics of InGaP/InGaAs double channel pseudomorphic high electron mobility transistors (DCPHEMTs) with graded and uniform triple δ-doped sheets were demonstrated and investigated. From simulated results, it was found that, the employed uniform triple δ-doped sheet profile did not perform as well as a graded triple δ-doped profile. In addition, simulations indicated that the device with graded triple δ-doped sheets shown high $g_{m,max}$ of 498 mA/mm, high $I_{D,max}$ of 177 mS/mm and good linearity properties. In addition, a practical DCPHEMT with graded triple δ-doped densities of $\delta_1(n^+) = 3 \cdot 10^{12}\,\mathrm{cm}^{-2}$, $\delta_2(n^+) = 2 \cdot 10^{12}\,\mathrm{cm}^{-2}$ and $\delta_3(n^+) = 1 \cdot 10^{12}\,\mathrm{cm}^{-2}$ was fabricated for comparison. Simulation data were in good agreement with experimental results. Furthermore, excellent microwave characteristic with flat and wide operation regime was also found. Consequently, the DCPHEMT with graded triple δ-doped sheets is shown to be promising for high performance digital and microwave device applications.

Acknowledgment: Part of this work was supported by the National Science Council of the Republic of China under Contract No. NSC-97-2221-E-006-238-MY3 and NSC-98-2221-E-006-238.

References

[1] M. Tomizawa, T. Furuta, K. Yokoyama, A. Yoshii. IEEE Trans. Electron Dev., **36**, 2380 (1989).
[2] W.S. Lour, M.K. Tsai, K.C. Chen, Y.W. Wu, S.W. Tan, Y.J. Yang. Semicond. Sci. Technol., **16**, 826 (2001).
[3] W.C. Liu, W.L. Chang, W.S. Lour, K.H. Yu, K.W. Lin, C.C. Cheng, S.Y. Cheng. IEEE Trans. Electron. Dev., **48**, 1290 (2001).
[4] C.S. Lee, C.H. Chen, J.C. Huang, K.H. Su. J. Electrochem. Sci., **154**, 374 (2007).

[5] N.H. Sheng, C.P. Lee, R.T. Chen, D.L. Miller, S.J. Lee. IEEE Electron. Dev. Lett., **6**, 307 (1985).
[6] T. Enoki, K. Arai, A. Kohzen, Y. Ishii. IEEE Trans. Electron. Dev., **42**, 1413 (1995).
[7] H.M. Chuang, S.Y. Cheng, C.Y. Chen, X.D. Liao, R.C. Liu, W.C. Liu. IEEE Trans. Electron. Dev., **50**, 1717 (2003).
[8] W.C. Hsu, H.M. Shieh, C.L. Wu, T.S. Wu. IEEE Trans. Electron. Dev., **41**, 456 (1994).
[9] M.J. Kao, W.C. Hsu, H.M. Shieh, T.Y. Lin. Solid-State Electron., **38**, 1171 (1995).
[10] S.I. Fu, R.C. Liu, S.Y. Cheng, P.H. Lai, Y.Y. Tsai, C.W. Hung, T.P. Chen, W.C. Liu, J. Vac. Sci. Technol. B, **25**, 691 (2007).
[11] S.Y. Cheng, K.Y. Chu, L.Y. Chen, L.A. Chen, C.Y. Chen, Appl. Phys. Lett., **90**, 043 5101 (2007).
[12] S.W. Tan, W.T. Chen, M.Y. Chu, W.S. Lour. Semicond. Sci. Technol., **19**, 167 (2004).
[13] H.M. Chuang, S.Y. Cheng, C.Y. Chen, C.H. Yen, X.D. Liao, R.C. Liu, W.C. Liu. Semicond. Sci. Technol., **19** 87 (2004).

Редактор Т.А. Полянская